Salffner, K.; Dönsberg, T.; Porrovecchio, Geiland; Smid, M.; Nield, K.; Nevas, Saulius

Characterization of a room temperature predictable quantum efficient detector for applications in radiometry and photometry

Published in:
Metrologia

DOI:
10.1088/1681-7575/aad19d

Published: 27/07/2018

Document Version
Publisher's PDF, also known as Version of record

Metrologia

PAPER • OPEN ACCESS

Characterization of a room temperature predictable quantum efficient detector for applications in radiometry and photometry

OPEN ACCESS
IOP Publishing | Bureau International des Poids et Mesures
Metrologia
Metrologia **55** (2018) 654–661
https://doi.org/10.1088/1681-7575/aad19d

Characterization of a room temperature predictable quantum efficient detector for applications in radiometry and photometry

K Salffner[1], T Dönsberg[2], G Porrovecchio[3], M Smid[3], K Nield[4,5] and S Nevas[1]

[1] Physikalisch-Technische Bundesanstalt, Bundesallee 100, 38116 Braunschweig, Germany
[2] Aalto University, PO Box 13000, 00076 Aalto, Finland
[3] Czech Metrology Institute, V Botanice 4, 150 72 Praha 5, Czechia
[4] Measurement Standards Laboratory of New Zealand, 69 Gracefield Road, Lower Hutt, New Zealand

E-mail: katharina.salffner@ptb.de

Received 19 April 2018, revised 27 June 2018
Accepted for publication 5 July 2018
Published 27 July 2018

Abstract

This paper presents the experimental characterization of predictable quantum efficient detectors, which have been designed for use at room temperature. The aim of the characterization was to validate modelled properties experimentally and, thus, the feasibility of such room temperature predictable quantum efficient detectors to be used as primary radiometric standards for applications in the fields of photometry and radiometry with an aimed uncertainty level of 0.01%. The characterizations were focused on linearity, thermal, angular, spectral and polarization dependencies of the detector that need to be known and considered in the respective applications. The results of the characterization measurements confirm the predictability of the detector, within the aimed 0.01% uncertainty level and, thus, the high potential for using that kind of devices as primary standards for applications in radiometry and photometry.

Keywords: characterization, radiometry, photometry, primary standard optical power, room-temperature quantum efficient detector (RT-PQED)

(Some figures may appear in colour only in the online journal)

1. Introduction

The concept of predicting internal quantum losses of a photodiode so that it can be used for the absolute measurement of optical power dates from the late 1970s [1]. Current silicon (Si)-based manufacturing technology together with the advancements in the computing capabilities and modelling of the charge carrier generation and dynamics processes allow the production of such photodiodes with the required characteristics. Hence, a predictable quantum efficient detector (PQED) based on induced junction silicon photodiodes was developed recently [2, 3]. Modelling and characterization at a set of selected wavelengths have shown that the spectral power responsivity of the produced PQED operated at room temperature can be predicted with a standard uncertainty at the level of 100 ppm (*parts per million* $= 1 \times 10^{-6}$, 100 ppm $= 0.01\%$) [2–5]. Thus, the developed PQED is to provide a cost-efficient and easy-to-use alternative to cryogenic radiometers. In terms of its handling complexity, the room temperature device (RT-PQED) is comparable to state-of-the-art transfer standard detectors (typically silicon trap detectors).

While implementing a novel primary radiometric standard for use at room temperature, the RT-PQED is of interest for various applications in photometry, filter radiometry and fibre optics [6]. In photometry, a successful application of

[5] Currently: International Commission on Illumination, Austria

the PQED was recently demonstrated in measurements of light-emitting diode (LED)-based light sources [7]. There, the RT-PQED replaced photometers that are normally used to measure photometric quantities of light sources. In that study, the PQED-based measurements lead to lower measurement uncertainties than the photometer-based measurements.

The RT-PQED equipped with a calibrated aperture can also be used as a primary standard for a direct calibration of photometers or filter radiometers with respect to their spectral irradiance responsivity, which offers a simpler calibration scheme compared to a typical traceability chain involving a cryogenic radiometer. However, the implementation of the RT-PQED as a primary standard for such applications in photometry and radiometry requires the experimental validation of the device under the measurement conditions generally faced during such applications: the optical radiation to be measured is uncollimated, has a varying degree of polarization and a finite bandwidth, i.e. it is not a monochromatic laser beam. Because of the anticipated spectral dependencies of the PQED properties, the performance of the RT-PQED with respect to the relevant measurement conditions must be validated over the whole spectral range relevant for the specific applications. Thus, the purpose of the characterization measurements presented in this paper was to characterize the RT-PQED performance focusing on effects and dependencies that are relevant and required for its successful implementation in radiometry and photometry applications. Here we present experimental methods used to determine the RT-PQED properties such as linearity, thermal, angular, spectral and polarization dependencies, along with the respective results obtained and discuss their implications for the applications of the device.

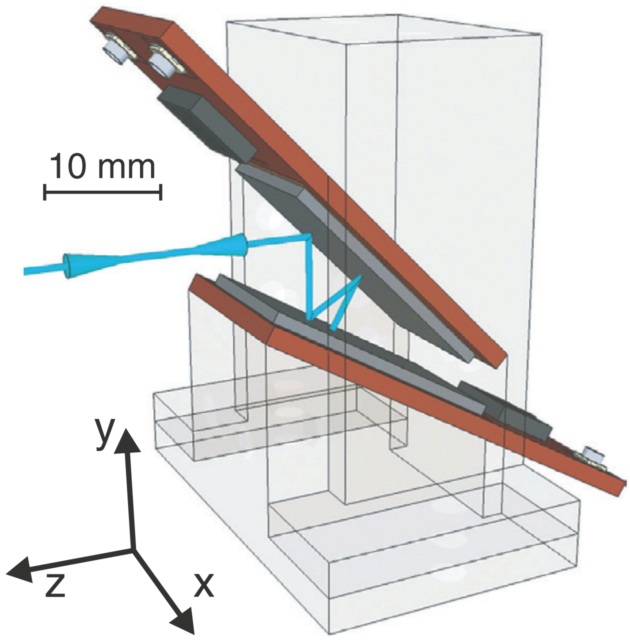

Figure 1. Schematic diagram of the PQED photodiodes assembly (Reproduced by [2]. © IOP Publishing Ltd. All rights reserved.) The blue arrows depict the incident beam. The beam undergoes seven absorptions and reflections at the photodiode surfaces before the remaining fraction of the beam exits through the entrance aperture.

2. Principle of the PQED

The spectral responsivity $s(\lambda)$ of a photodiode can be written as

$$s(\lambda) = \frac{e \cdot \lambda}{h \cdot c} \cdot [1 - \rho(\lambda)] \cdot [1 - \delta(\lambda)] \cdot [1 + \gamma(\lambda)] \quad (1)$$

where e and c are the fundamental physical constants of the elementary charge and speed of light in vacuum, h is the Planck constant and λ is the wavelength. The other terms account for spectrally dependent reflectance losses (ρ), internal quantum deficiencies in the photodiode (δ) and internal charge carrier gain (γ). These terms are relative values and therefore dimensionless. For Si-based photodiodes, the effect of internal charge carrier gain $\gamma(\lambda)$ mainly becomes relevant at wavelengths in the UV spectral range.

The approach to the PQED design includes two aspects: the design of the photodiode structure leading to minimized quantum deficiency in the bulk of the photodiode and the design of the geometry of the photodiode assembly allowing the reflections to be trapped and the losses to be reduced down to a level of 10 ppm.

The developed RT-PQED is based on induced junction photodiodes showing very low internal quantum deficiencies $\delta(\lambda)$ [2, 3]. A bias voltage, typically 5 V, is applied to the photodiodes to further reduce internal losses [8]. The dependence of the RT-PQED response on the bias voltage has been investigated experimentally by Müller *et al* [3]. The bias voltage dependence of the internal quantum deficiency has been modelled and measured by Tang *et al* [9].

The RT-PQED uses two photodiodes arranged in a wedge of 15° (figure 1). In this alignment, an incident beam undergoes seven in-plane reflections between the two photodiodes before it leaves the RT-PQED co-linearly to the incoming beam, similarly to corner cube-configured trap detectors. Consequently, the remaining fraction of the beam power that leaves the detector is very low. Depending on the wavelength, the reflectance $\rho(\lambda)$ of the RT-PQED assembly is modelled to be in the range of a few ppm to a few hundred ppm [10]. The modelled values for the reflectance have been confirmed at a set of wavelengths [2].

A more detailed description of the semiconductor material and assembly design is given in [2, 3].

3. Characterization of the RT-PQED

3.1. Linearity and dynamic range

The dynamic range of a photodiode is determined at the upper end by the nonlinearity effect due to the saturation of the conversion of the photons to charge carriers. At the lower end, this dynamic range is determined by both the noise and by the dark current generated by the photodiode [11]. The saturation point of an RT-PQED is dependent on the bias voltage applied to the photodiodes and the spatial photon density of the optical radiation impacting the photodiodes [12]. The dark

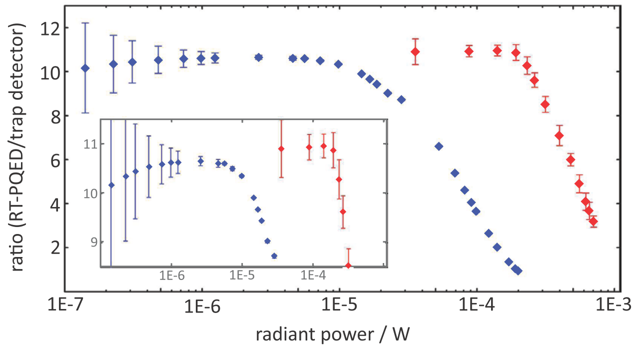

Figure 2. Saturation levels with unbiased (blue) RT-PQED and bias of 5 V (red). The insert shows a zoom of the graph. The *y*-axis gives the ratio of the photocurrents measured by the RT-PQED and the trap detector, the latter one being hit by approx. 1/10 of the power impinging on the RT-PQED. The error bars represent the type A uncertainty of 20 repeated measurements.

photocurrent is dependent on the bias voltage and on the photodiode temperature.

The saturation level of an RT-PQED was experimentally determined by measuring the ratio between the photocurrent of an RT-PQED and that of a three-element Si-based trap detector of known linearity over 5 decades of optical power. This experiment was performed with and without bias voltage being applied to the RT-PQED.

The incident irradiation used in these experiments consisted of a stabilized (50 ppm h^{-1}) quasi-Gaussian laser beam with a $1/e^2$ diameter of 3 mm and a wavelength of 531 nm. The value of the laser beam diameter has been chosen as a trade-off between distributing its energy on the largest area over the photodiodes to decrease the photon density level and limiting the loss of optical radiation due to the size of the RT-PQED circular aperture of 8 mm diameter. A beam splitter with a ratio of about 1 : 10 was used to distribute the optical radiation between the two detectors with the weaker beam impacting the trap detector.

The range of laser power, over which the measurements were made, was obtained by using the dynamic range of the laser stabilization system in conjunction with a graduated neutral density filter. With the presence of the beam splitter in the optical path of the beam conjoiner apparatus, this resulted in the combined, incident optical radiation power at both the trap detector and the RT-PQED ranging from approx. 140 nW to 0.7 mW. Considering the beam diameter of 3 mm, the equivalent irradiance levels range from 0.015 W m^{-2} to 74 W m^{-2}. As mentioned above, the trap detector is hit by 1/10 of this power. Thus, this is well within the linearity range of the trap detector, which has been verified from 40 pW to 1 mW using the dual beam addition technique [12, 13].

As expected [2, 3], the unbiased RT-PQED already shows nonlinear behaviour at rather low power levels (10 μW). The non-linearity threshold for this evaluation was chosen at as high as 100 ppm, which was the typical level of uncertainty of this measurement. The linear performance of the RT-PQED is extended to higher power levels (200 μW) if the 5 V bias voltage is applied to the photodiodes (figure 2).

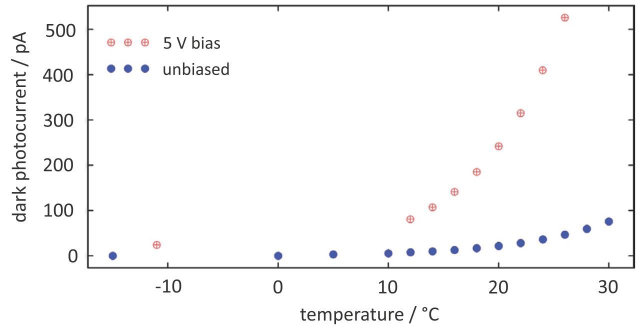

Figure 3. Temperature dependence of the RT-PQED dark photocurrent when the RT-PQED is operated with 5 V bias and in unbiased mode.

3.2. Temperature dependence of the dark photocurrent and noise

The temperature dependence of the dark photocurrent and noise characteristics were measured with the RT-PQED held in light tight conditions. A custom-made heat pipe temperature controller was developed for the temperature characterization of the RT-PQED [14]. Using this controller, measurements could be made from −12 °C to 35 °C, with a stability at each set point of ±0.02 °C. The RT-PQED was purged with dry gas to avoid condensation on the photodiodes below the ambient dew-point temperature.

The dark photocurrent was measured by using a transimpedance amplifier with a feedback resistor of 1 GΩ. As shown in figure 3, within the temperature range of −12 °C to 30 °C, the dark photocurrent depends exponentially on the temperature of the RT-PQED. When a voltage bias of 5 V is applied, the dark photocurrent is one order of magnitude larger than if no external bias is used. These trends of the dependence on the temperature and bias voltage are as expected. Former measurements of the dark photocurrent of a PQED of the same type[6] with 5 V bias applied [15] resulted in a higher dark photocurrent at room temperature (approx. 10 nA at 24 °C). A probable reason is a slight change in the photodiode material occurring between different batches of the photodiode production.

The need to minimize the dark photocurrent when measuring low radiance flux levels is apparent. Firstly, at room temperature and when a 5 V bias is applied, this limits the I/V factor of the transimpedance amplifier that can be used to measure the RT-PQED photocurrent down to 1×10^{-10} A before the readout electronics saturate. Secondly, when the dark photocurrent is higher, the thermally dependent fluctuations also increase, especially when operated without temperature control.

The RT-PQED noise was measured at different temperatures using a switched integrating amplifier (SIA) [16] with a gain of $1 \times 10^{+10}$ V A^{-1}. The noise bandwidth of the SIA is well defined [11] and is equal to 1/2 τ, where τ is the integration time of the SIA. During this measurement, the SIA integration time was 1 s and no bias voltage was applied to

[6] Dönsberg *et al* focuses on PQED based on photodiodes with *n*-type silicon substrate and compares them to *p*-type-based PQED. The measurements presented here in this paper are carried out with *p*-type-based PQED.

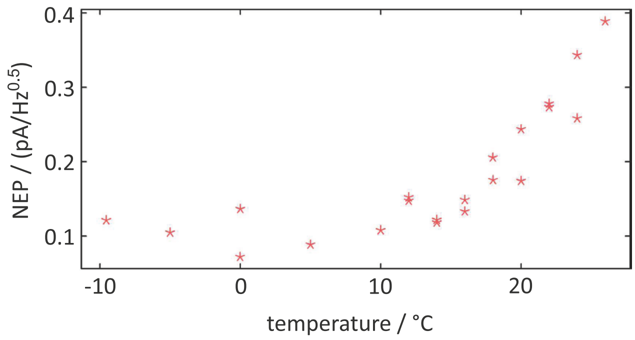

Figure 4. Temperature dependence of the RT-PQED noise equivalent power (NEP) measured with a switched integrator amplifier at $1 \times 10^{+10}$ gain and no bias voltage applied to the photodiodes.

the RT-PQED photodiodes. The results of this measurement are shown in figure 4. Below 5 °C there is no further measurable noise reduction probably due to the electronics noise floor being the dominant contribution.

The collected experimental data from the RT-PQED linearity, dark signal and noise performance suggest the use of the RT-PQED in two regimes depending on the intended measurement mode and irradiance level to be measured: (i) with applied bias voltage to measure power levels as are typical for current absolute primary standard radiometers (>approx. $1\,W\,m^{-2}$ or approx. 10 μW for a beam with a 3 mm diameter), and (ii) unbiased and possibly temperature-stabilized PQED to about 10 °C to provide measurements of optical power down to very low photon fluxes.

3.3. Angular dependence

The dependence of the RT-PQED responsivity on the angle of incidence of a beam must be known for radiometric and photometric applications involving radiation sources with non-collimated beams, such as incandescent light bulbs or LEDs. Based on the modelling presented in [2, 3], no effects larger than a few ppm were expected for the angular-dependent measurements.

To characterize the angular dependence of the RT-PQED responsivity, a power-stabilized, collimated and linearly polarized laser beam was used. The laser system is described in [17]. The measurements were carried out at four wavelengths: 400 nm, 515 nm, 680 nm, and 800 nm. Figure 5 gives a schematic diagram of the optical setup of these measurements.

The spatial profile and beam quality of the laser was optimized by using a spatial filter. The optimum beam shape for the angular and uniformity measurements would be a flat-top, because of its steep edges that cause less unwanted effects of beam walking than the broader edges of a Gaussian beam. Nevertheless, to achieve a flat-top beam with sufficient contrast ($>1 \times 10^{+4}$), a high loss of laser power would have been the consequence. Therefore, the spatial filter was adjusted to achieve a Gaussian-like beam profile. Knife-edge measurements along two orthogonal directions showed no significant differences for the beams at the different wavelengths within the standard deviation of these measurements. The beam radii

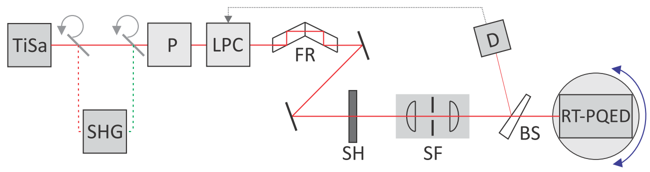

Figure 5. Schematic diagram of the optical setup of the angular dependence measurements. The red and green lines depict the optical path from the two laser sources. The RT-PQED was placed on a rotary table. TiSa—titanium-sapphire laser, SHG—second harmonic generator, P—polarizer, LPC—laser power controller, FR—Fresnel rhomb, SH—shutter, SF—spatial filter, BS—beam splitter, D—feedback diode.

($1/e^2$) were between 0.7 mm and 0.9 mm. The power level of the laser was below 60 μW and a bias voltage of 5 V was applied to the RT-PQED photodiodes.

To measure the angular dependence in two orthogonal planes, the RT-PQED was rotated around the x- and y-axes (figure 1) which are in plane with the entrance aperture of the detector (approximately 40 mm in front of the photodiodes assembly). This position for the rotational axis has been chosen as the intention of this measurement was to estimate the acceptable divergence angle of a radiation field that could be measured with the RT-PQED fitted with an apperture for radiometric or photometric applications.

The measurements were done from $+3°$ to $-3°$ angular displacement, where angular displacement means the angle spanning between the optical axis of the laser beam and the virtual optical axis within the RT-PQED as shown by the blue arrows in figure 1.

The photocurrents of the two photodiodes were measured individually. For the analysis of the data, the values of the photocurrents measured from the two photodiodes are summed, corrected for dark signal and drift and compared to the measurement at 0° angular displacement.

Figure 6 shows the results from the angular-dependence measurements. For the measurements at 515 nm and 680 nm, only slight signal deviations are observed which are within the aimed uncertainty range of 100 ppm. The results of the measurements at 400 nm and 800 nm show larger variations.

One possible cause of this behaviour could be the wavelength-dependent reflectance of the RT-PQED. At around 400 nm, the reflectance increases rather steeply, so changes of e.g. ±0.5 nm of the centre wavelength during the measurement could cause changes in the reflectance and thereby measured signal of approx. 50 ppm[7] [10]. At around 680 nm and 800 nm the change of reflectance would be an ordner of magnitude lower if the wavelength changed by ±0.5 nm. At around 515 nm, the change in reflectance would even be below 1 ppm.

Further possible reasons for the—in this case alleged—wavelength dependency of the angular dependence are the quality of the beam shape and spatial (non-)uniformity of the RT-PQED's responsivity. In combination with the movement

[7] Prior to the measurements, the laser had been tuned to the particular center wavenlength. During the measurements the laser wavelength was not monitored. Changes of the center wavelength can, therefore, not be excluded.

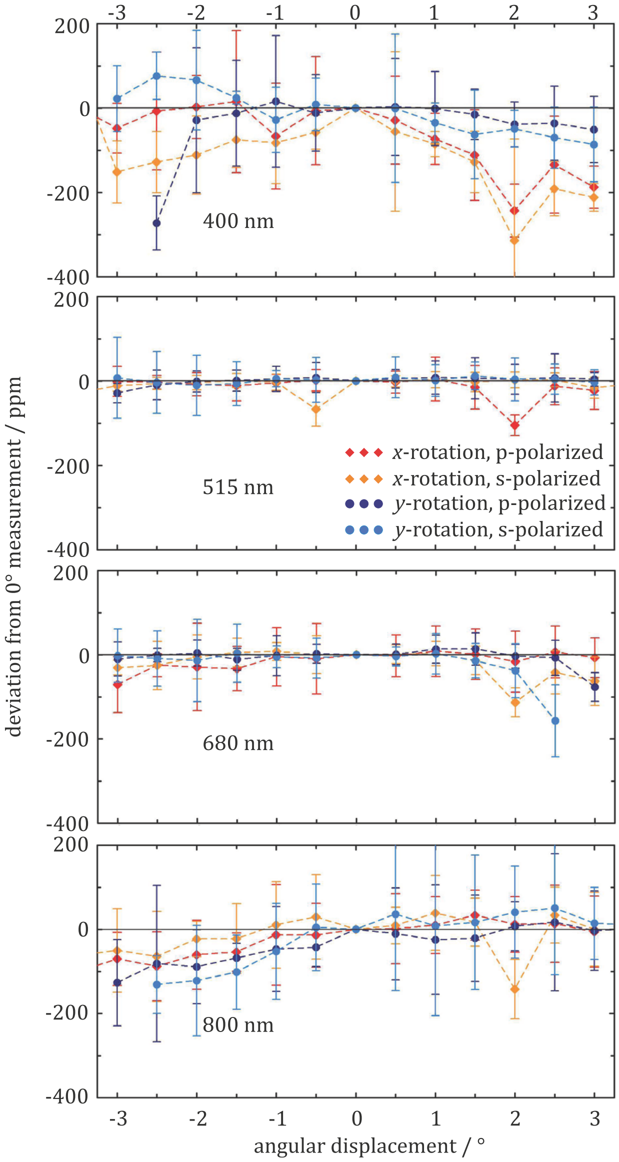

Figure 6. Results of the angular-dependence measurements. The relative deviation of the measured photocurrent as a function of angular displacement from the center position (0°) is given. The blue bullets show the results from the rotation around the *y*-axis ('*y*-rotation') for the s-polarized (light blue) and the p-polarized (dark blue) beam. The diamonds show the results from the rotation around the *x*-axis ('*x*-rotation') for the s-polarized (orange) and the p-polarized (red) beam. The error bars represent the type A uncertainty of five repeated measurements.

of the beam across the photodiode area during the angular dependence measurements, this could cause results as seen in figure 6.

The spatial uniformity of the responsivity of this RT-PQED has been measured before [18] at a different optical setup. For these measurements, a circular area of approx. 6 mm times 6 mm has been scanned with a laser beam at $\lambda = 488$ nm. The $1/e^2$ beam diameter was approx. 1.2 mm and the laser power approx. 200 μW. A bias voltage of 5 V has been applied to the RT-PQED photodiodes. The responsivity changes across the scanned area are below 100 ppm. So the uniformity is less likely to cause the variations in the angular dependence measurements.

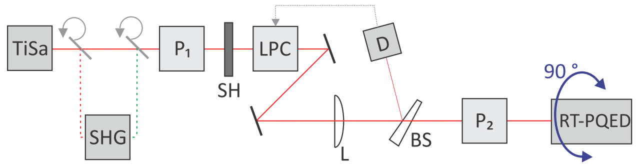

Figure 7. Schematic diagram of the optical setup of the polarization dependence measurements. The red and green lines depict the optical path from the two laser sources. The RT-PQED was attached to a special rotation unit to ensure that the RT-PQED is rotated around the optical axis without moving the beam along the RT-PQEDs photodiodes surfaces. TiSa—titanium-sapphire laser, SHG—second harmonic generator, P—polarizers, SH—shutter, LPC—laser power controller, L—lens with $f = 800$ mm, BS—beam splitter, D—feedback diode.

Even though the spatial profile of the beam has been tested by simplified knife-edge measurements, it cannot be excluded that there were artefacts in the beam quality, which might lead to these deviations of around 100 ppm.

Nevertheless, the observed deviation of the signal as a function of angular displacement is rather low and at the level of around 100 ppm for angles $\pm 2°$ throughout the investigated spectral range from 400 nm to 800 nm. Regarding the initial motivation to estimate the acceptable divergence angle of a radiation field, a maximum divergence of 2° is therefore recommended.

3.4. Polarization dependence

As mentioned before, the general approach of the RT-PQED is to minimize any external and internal losses. Nevertheless, although the multiple absorption between the two photodiodes significantly reduces losses by reflection, the remaining losses are still in the range of a few ppm up to few hundreds of ppm, depending on the wavelength. Therefore, a correction is needed for these remaining losses. The expected values for the remaining reflectance were calculated by Sildoja *et al* [10] as a function of wavelength and the state of polarization of the light source.

To validate these calculations and thereby the feasibility of the correction, the polarization dependence of the responsivity of the RT-PQED was tested at different wavelengths. For this experiment, a laser beam with highly linear polarization was used and the RT-PQED was rotated around the optical axis of the laser beam (z in figure 1) to change the relative orientation between the laser beam polarization of the laser beam and the photodiode surfaces of the RT-PQED. Figure 7 gives a schematic diagram of the optical setup that was used for the polarization dependence measurements.

Figure 8 shows the course of the summed photodiodes signals as the RT-PQED is rotated, with the example of the laser wavelength being 680 nm. As expected, the signal decreases when the polarization of the beam changes from p to s, as the reflectance is higher for s-polarized light leading to higher losses.

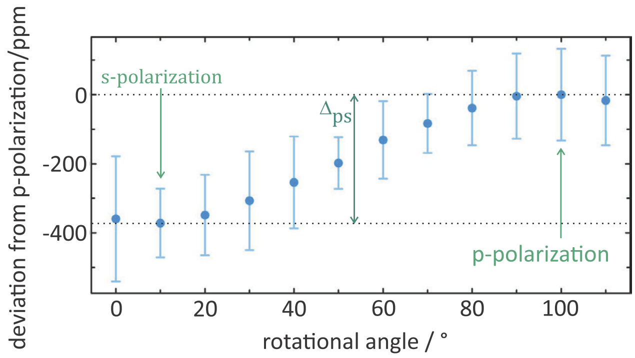

Figure 8. Deviation of the measured photocurrent for the rotation of the RT-PQED around the optical axis ($\lambda = 680$ nm). The error bars represent the type A uncertainty.

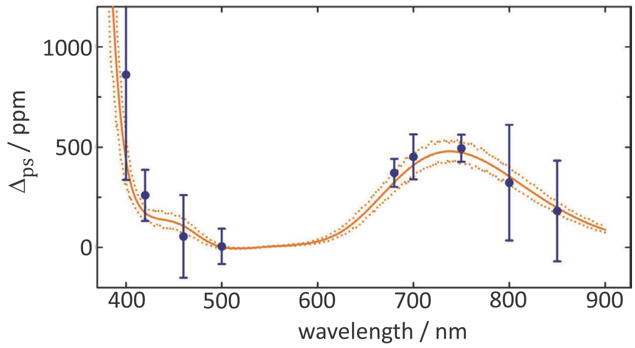

Figure 9. Calculated values of the difference between signals from p- and s-polarized radiation (Δ_{ps}). The experimentally determined values are given in blue bullets. The error bars represent the type A uncertainty. The modelled values as calculated by Sildoja *et al* [10] are given as a solid orange line. The dotted lines represent the uncertainty of the modelled values.

To compare our experimental results to expected values from the modelling by Sildoja *et al* [10], the relative difference Δ_{ps} between the signals measured with s- and p-polarized light was calculated and compared to the expected difference of reflection for s- and p-polarized light. Figure 9 shows Δ_{ps} as a function of the wavelength as determined experimentally (blue bullets) in comparison to the expected values based on the modelling (orange line). The experimental values are in agreement with the modelled values within the uncertainty of the model and the experiment.

3.5. Bandwidth dependence

As it applies to any other reference detector, the course of the spectral responsivity $s(\lambda)$ of the RT-PQED with wavelength λ and, thus, the bandwidth dependence of an RT-PQED signal must be accounted for when it is used to calibrate a radiometric or photometric detector. For such calibrations, both detectors (reference and device under test) are irradiated with radiation of finite bandwidth. If the spectral responsivity $s(\lambda)$ of a detector varies nonlinearly within the bandwidth of the radiation, the apparent spectral responsivity of this detector will be bandwidth dependent.

Figure 10 shows a scheme to illustrate this effect. If $s(\lambda)$ shows linear behaviour (dashed blue line), the measured responsivity will not depend on the spectral bandwidth of the incident optical radiation. For a nonlinear course of the spectral responsivity (dotted red line), measurements with a spectral bandwidth of 1 nm would mistakenly lead to lower values for the measured responsivity around the centre wavelength λ_0 as measurements with a 0.1 nm bandwidth.

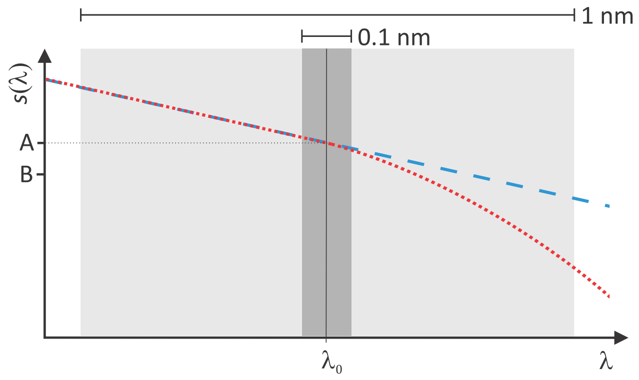

Figure 10. Schematic diagram to illustrate the bandwidth dependence caused by nonlinear variation of a photodiode's spectral responsivity $s(\lambda)$. The blue and red curves show possible courses of this spectral responsivity. The marks A and B represent estimated values of $s(\lambda_0)$ that would be determined with a bandwidth of 0.1 nm (A) or 1.0 nm (B).

To experimentally test the bandwidth dependence of the RT-PQED, the irradiance E_{PQED} measured by the RT-PQED was compared to the irradiance measured by a reference trap detector E_{ref}. The spectral responsivity of this reference trap detector is traced back to the cryogenic radiometer and the bandwidth dependence of this reference detector is sufficiently known. The bandwidth $\Delta\lambda$ of the radiation sources used was limited by a monochromator to 0.1 nm, 0.3 nm, 1 nm, 1.5 nm, 5 nm and 10 nm. The measurements were taken at around 500 nm, 700 nm and 900 nm. For each spectral range, the irradiance was measured at three wavelengths 1 nm apart. The tuning of the wavelength was performed to additionally check for a possible effect of $\mathrm{d}s(\lambda)/\mathrm{d}\lambda$ in combination with the different bandwidths. Figure 11 gives a schematic diagram of the optical setup that was used for these measurements.

The three centre wavelengths were chosen due to the progression of the spectral responsivity $s(\lambda)$ of the RT-PQED. As can be seen in equation (1), the spectral responsivity $s(\lambda)$ is the sum of the linear term based on the photoelectric effect and the potentially nonlinear losses induced by reflection ($\rho(\lambda)$) and internal quantum deficiencies ($\delta(\lambda)$). At around 500 nm, losses by reflection are at a minimum [10] and the course of $s(\lambda)$ is expected to be rather linear. At around 700 nm, the reflection losses increase, which might lead to nonlinear behaviour of $s(\lambda)$ and thereby bandwidth dependency. At around 900 nm, reflection losses decrease and losses by internal quantum deficiencies are at a high and increasing level [9], which also might lead to the nonlinear behaviour of $s(\lambda)$. The spectral responsivity of the reference trap detector is known to be linear in all these three spectral ranges.

Figure 12 shows the results for the measurements at around 700 nm and bandwidths of 0.1 nm, 0.3 nm and 1 nm. The graph shows the deviation of the ratio $E_{\mathrm{ref}}/E_{\mathrm{PQED}}$ compared to the particular mean value of $E_{\mathrm{ref}}/E_{\mathrm{PQED}}$. The error bars represent the standard deviation from the mean of five to twenty

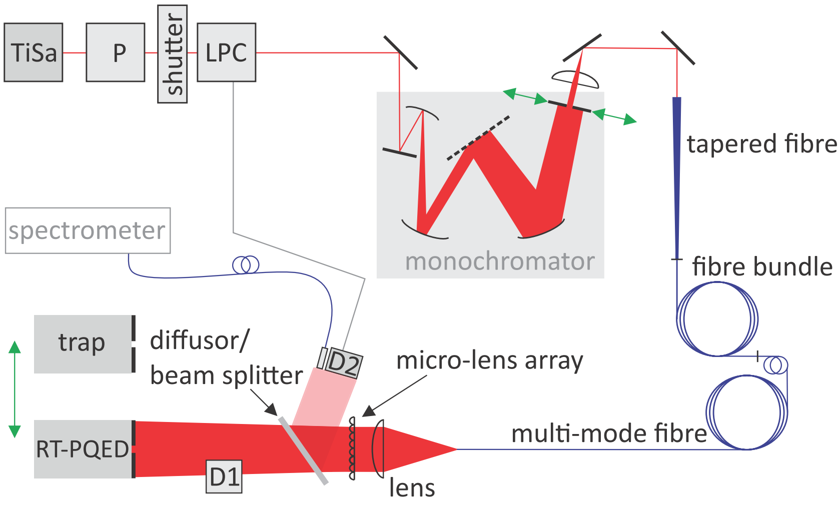

Figure 11. Schematic diagram of the optical setup of the bandwidth-dependent measurements. The red lines depict the open optical path. The spectral bandwidth was limited by the width of the monochromators exit slit. TiSa—titanium-sapphire laser, P—polarizer, LPC—laser power controller, D1—monitor photodiode, D2—feedback diode of the LPC.

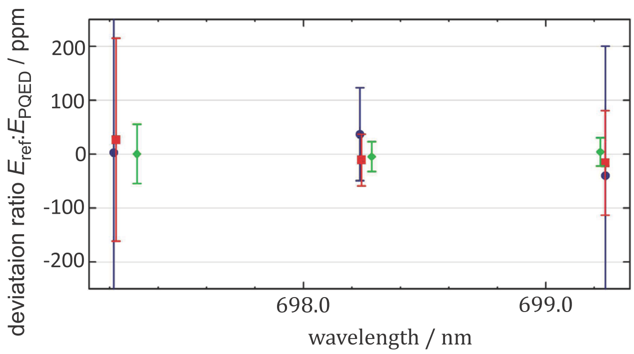

Figure 12. Deviation of the ratio of the irradiance E_{ref} measured with the reference detector and E_{PQED} measured with the RT-PQED. The spectral bandwidth was set to 0.1 nm (blue circle), 0.3 nm (red square), and 1 nm (green diamond). The error bars represent the type A uncertainty.

repeated measurements. The rather low optical power behind the monochromator for the 0.1 nm bandwidth measurement leads to a deterioration in signal-to-noise ratio.

As can be seen in figure 12, the irradiance ratios measured with the reference trap detector and the RT-PQED are in agreement within the associated standard deviation for all bandwidths and the stepwise scanned wavelength range. The measurements with higher bandwidths and at the other wavelengths revealed the same results. That means, no indication for bandwidth dependence of the RT-PQED spectral responsivity has been observed for the investigated spectral ranges (around 500 nm, 700 nm and 900 nm) and for bandwidths ranging from 0.1 nm to 10 nm.

4. Discussion and conclusion

This paper presented results from the experimental characterization of predictable quantum efficient detectors that are used at room temperature. The aim of the measurements was to investigate the linearity of the responsivity, the dark signal and the noise performance of the RT-PQED, and to validate modelling results of the RT-PQED performance. This validation was done with regard to polarization-, angular- and bandwidth-dependent performance. The overall aim of these measurements was to investigate the feasibility of the RT-PQED to be used as a primary standard for optical power with the focus on applications in photometry and radiometry.

The responsivity of the RT-PQED photodiodes becomes nonlinear at irradiance levels around 1 W m^{-2}. To extend the range of linear performance, a bias voltage can be applied to the photodiodes. In the case of a 5 V bias, the linear range of the responsivity is extended to about 40 W m^{-2} and could be further extended by higher bias voltages for applications with higher radiant power. As is commonly expected, the bias voltage increases the dark photocurrent of the RT-PQED photodiodes. If no bias voltage is applied, the dark photocurrent is comparable to standard trap detectors and the noise equivalent power is below 1×10^{-9} A Hz$^{-0.5}$ and even 1×10^{-10} A Hz$^{-0.5}$ if the RT-PQED is cooled to temperatures below 10 °C. To summarise, the dynamic range of the RT-PQED was characterised in two regimes: the detector biased with 5 V voltage and unbiased. The signal-to-noise-ratio of $1 \times 10^{+4}$ under 1 s integration time was used to define the lower limit of the dynamic range while its upper limit was defined by its non-linearity reaching the level of 100 ppm. In biased (5 V) regime, the resulting dynamic range of the RT-PQED spans from 0.07 W m^{-2} to 40 W m^{-2} while the dynamic range in the unbiased mode is from 70 μW m^{-2} to 0.4 W m^{-2}.

The experimental results from the polarization-dependence measurements agree with the predictions by modelling within the aimed uncertainty level of 100 ppm. The bandwidth-dependent measurements revealed no significant bandwidth dependence. The RT-PQED showed angular dependence at some wavelengths which was not expected. Possible reasons for this performance are the wavelength-dependent reflectance or the beam quality, even though it was optimized. Nevertheless, the observed angular dependence of the RT-PQED does not exceed the level of 100 ppm for incident angles $\pm 2°$ for all measured wavelengths. Therefore, it is regarded to be negligible for applications with radiation fields of a divergence lower than 2°, which is fulfilled by most of the standard photometric and radiometric applications.

The results from all these characterization measurements are a strong indication of the predictability of such a detector, within the aimed 100 ppm uncertainty level. Overall, the results presented in this paper are promising for the use of RT-PQED as an easy-to-use and cost-efficient primary standard for optical power. The results from the investigation of the RT-PQEDs polarization, angular and bandwidth dependence show the high potential for using the RT-PQED as a primary standard for applications in radiometry and photometry.

Acknowledgment

The research work leading to this article was carried out within the EMRP SIB57 Project 'New primary standards and traceability for radiometry'. The EMRP is jointly funded by the EMRP participating countries within EURAMET and the European Union.

ORCID iDs

K Salffner https://orcid.org/0000-0002-3354-494X
T Dönsberg https://orcid.org/0000-0002-7783-4244

References

[1] Geist J 1979 Quantum efficiency of the p–n junction in silicon as an absolute radiometric standard *Appl. Opt.* **18** 760–2
[2] Sildoja M, Manoocheri F, Merimaa M, Ikonen E, Müller I, Werner L, Gran J, Kuebarsepp T, Smid M and Rastello M L 2013 Predictable quantum efficient detector: I. photodiodes and predicted responsivity *Metrologia* **50** 385–94
[3] Müller I *et al* 2013 Predictable quantum efficient detector: II. Characterization and confirmed responsivity *Metrologia* **50** 395–401
[4] Sildoja M, Manoocheri F and Ikonen E 2009 Reflectance calculations for a predictable quantum efficient detector *Metrologia* **46** 151–4
[5] Gran J, Kuebarsepp T, Sildoja M, Manoocheri F, Ikonen E and Mueller I 2012 Simulations of a predictable quantum efficient detector with pc1d *Metrologia* **49** 130–4
[6] Newstar—new primary standards and traceability for radiometry (project SIB 57 within the European Metrology Research Programm EMRP)
[7] Dönsberg T, Pulli T, Poikonen T, Baumgartner H, Vaskuri A, Sildoja M, Manoocheri F, Kaerhae P and Ikonen E 2014 New source and detector technology for the realization of photometric units *Metrologia* **51** 276–81
[8] Geist J, Lang E and Schaefer A R 1981 Complete collection of minority carriers from the inversion layer in induced junction diodes *J. Appl. Phys.* **52** 4879–81
[9] Tang C K, Gran J, Müller I, Linke U and Werner L 2015 Measured and 3d modelled quantum efficiency of an oxide-charge induced junction photodiode at room temperature *NUSOD* (IEEE) https://doi.org/10.1109/NUSOD.2015.7292880
[10] Sildoja M, Dönsberg T, Maentynen H, Merimaa M, Manoocheri F and Ikonen E 2014 Use of the predictable quantum efficient detector with light sources of uncontrolled state of polarization *Meas. Sci. Technol.* **25** 015203
[11] Porrovecchio G, Smid M, Mountford J, Cheung J, Chunnilall C and White M Sub pw absolute light radiation measurement technique with trap detector and switched integrator amplifier publication under preparation
[12] Boivin L P 1993 Automated absolute and relative spectral linearity measurements on photovoltaic detectors *Metrologia* **30** 355–60
[13] Nield K, Porrovecchio G and Smid M (ed) 2010 Evaluation of the linearity performance of silicon trap detectors with switch integrator amplifiers at low optical powers *Proc. CIE Symp. II (Bern, September 2010)*
[14] Nield K, Mason R, Rougie B, Renoux D, Edgar H and Smid M 2014 Heat-pipe temperature controller system for the room temperature predictable quantum efficient detector *Proc. of NEWRAD (2014)*
[15] Dönsberg T *et al* 2017 Predictable quantum efficient detector based on n-type silicon photodiodes *Metrologia* **54** 821–36
[16] Mountford J, Porrovecchio G, Smid M and Smid R 2008 Development of a switched integrator amplifier for high-accuracy optical measurements *Appl. Opt.* **47** 5821–8
[17] Schuster M, Nevas S, Sperling A and Voelker S 2012 Spectral calibration of radiometric detectors using tunable laser sources *Appl. Opt.* **51** 1950–61
[18] Dönsberg T, Sildoja M, Manoocheri F, Merimaa M, Petroff L and Ikonen E 2014 A primary standard of optical power based on induced-junction silicon photodiodes operated at room temperature *Metrologia* **51** 197–202